ACCEPTED VERSION

D. J. Arnold, Y. M. Stokes, and J. E. F. Green
Thin-film flow in helically wound shallow channels of arbitrary cross-sectional shape
Physics of Fluids, 2017; 29(1): 013102-1-013102-11

© 2017 AIP Publishing

Originally published at: http://dx.doi.org/10.1063/1.4973670

PERMISSIONS

https://publishing.aip.org/authors/web-posting-guidelines

Web posting guidelines for papers in AIP Journals and Proceedings

Under the terms of its License to Publish Agreement,* AIP Publishing grants to the Author(s) of papers submitted to or published in one of AIP Publishing's journals or conference proceedings the following rights:

On the authors' personal web page and employers' web page:

The right to:

- Post the Accepted Manuscript (AM) to their personal web page or their employer's web page immediately after acceptance by AIP Publishing.
- Post the Version of Record (VOR) to their personal web page or their employer's web page 12 months after publication by AIP Publishing.

(An appropriate credit line must be included that references the full citation for the published paper, along with a link to the VOR after publication on AIP Publishing's site.)

In an institutional or funder-designated repository (i.e. PubMed):

The right to:

- Deposit the AM in a repository in compliance with university or funder requirements immediately after acceptance by AIP Publishing.
- Deposit the VOR in a repository in compliance with university or funder requirements 12 months after publication by AIP Publishing.

(An appropriate credit line must be included that references the full citation for the published paper, along with a link to the VOR after publication on AIP Publishing's site.)

11 May 2017

http://hdl.handle.net/2440/105081

This manuscript was accepted by Phys. Fluids. Click here to see the version of record.

Thin-film flow in helically-wound shallow channels of arbitrary cross-sectional shape

D. J. Arnold,[1,2] Y. M. Stokes,[2] and J. E. F. Green[2]
[1)] *Department of Mathematics, University of California Los Angeles, Los Angeles, CA 90095, USA*
[2)] *School of Mathematical Sciences, The University of Adelaide, Adelaide, SA 5005, Australia*

(Dated: 20 December 2016)

We consider the steady, gravity-driven flow of a thin film of viscous fluid down a helically-wound shallow channel of arbitrary cross-sectional shape with arbitrary torsion and curvature. This extends our previous work[1] on channels of rectangular cross section. The Navier-Stokes equations are expressed in a novel, non-orthogonal coordinate system fitted to the channel bottom. By assuming that the channel depth is small compared to its width and that the fluid depth in the vertical direction is also small compared to its typical horizontal extent, we are able to solve for the velocity components and pressure analytically. Using these results, an ODE for the free surface shape is obtained, which must in general be solved numerically. Motivated by the aim of understanding flows in static spiral particle separators used in mineral processing, we investigate the effect of cross-sectional shape on the secondary flow in the channel cross-section. We show that the competition between gravity and inertia in non-rectangular channels is qualitatively similar to that in rectangular channels, but that the cross-sectional shape has a strong influence on the breakup of the secondary flow into multiple clockwise-rotating cells. This may be triggered by small changes to the channel geometry, such as one or more bumps in the channel bottom that are small relative to the fluid depth. In contrast to the secondary flow which is quite sensitive to small bumps in the channel bottom, the free-surface profile is relatively insensitive to these. The sensitivity of the flow to the channel geometry may have important implications for the design of efficient spiral particle separators.

ACCEPTED MANUSCRIPT

I. INTRODUCTION

Fluid flows in helical geometries are of interest both in biology, *e.g.* in the circulatory system[2–4] or in the cochlea[5], and in industrial applications. An important example of the latter are flows in spiral particle separators — devices used in the mining and mineral processing industries to separate ores and clean coal[6–11]. They consist of a helically wound channel, typically with a curved bottom, down which a slurry of mixed particles and water flows. The depth of the channel is typically small compared to its width, i.e. the channels are shallow. As the slurry flows down the channel, the particles tend to separate across the width of the channel according to their weight, so that, in principle, at the outlet of the channel the flow can be split into separate streams each containing one type of particle. More recently, biomedical researchers have designed microfluidic devices consisting of closed spiral ducts which aim to use the same principles to separate circulating tumour cells from the blood[12].

Whilst spiral particle separators have been widely used for many years, and academic interest dates back to experimental work by Holland-Batt [6,7], mathematical modelling of the flow in them has been limited, and the design process is based mainly on experimentation; see Holland-Batt [8] for a summary. Experimental and numerical investigations into the flow have been undertaken, and empirical formulae derived to fit observed data. However, many of these studies have made quite restrictive assumptions: for example, a model developed by Holland-Batt [7] assumed a Manning law in the inner region of the channel, and a free vortex in the outer region. Validating these assumptions, and experimentation in general, has proven difficult, with experimental errors in measurement of flow velocities estimated to be as high as 30%. Nevertheless, a series of experiments[11,13,14] showed that a complex secondary flow exists, that a fully-developed steady state flow profile appears relatively quickly (within 2–3 turns down the spiral), and that the fluid depth is typically very shallow (1–12mm) relative to the channel width (250–350mm). Recently, Boucher *et al.*[15,16] performed experiments using positron emission particle tracking to obtain more information about the motion of particles in spiral separators, but their techniques did not allow measurement of the vertical component of the particle velocity, the free-surface shape or the bulk flow. Computational simulations of particle-free flow have been performed[17–19] and of dilute particulate flow where the particles are assumed not to modify the particle-free flow[20].

The aim of all of the above studies is to obtain an improved quantitative understanding of fluid flows in spiral separators to assist in their design. Thus the effects of geometrical factors such as curvature, torsion and cross-sectional profile on the flow are of particular interest. Motivated by these applications, recent work has considered the idealised problem of free surface flow of Newtonian fluid in a helically wound channel[21]. To our knowledge these authors were the first to exploit the fact that the depth of fluid in the separator is typically small relative to the

This manuscript was accepted by Phys. Fluids. Click here to see the version of record.

channel width, which allowed them to use the thin-film approximation to obtain a reduced model for the flow. Their study was restricted to helically symmetric flows in rectangular channels with small curvature and torsion, but in this regime they were able to demonstrate good agreement between their thin-film model and the results of numerical simulations of the full helically-symmetric Navier-Stokes equations. Subsequently, this thin-film model was extended to the case of rectangular channels of arbitrary curvature and torsion by Arnold, Stokes, and Green [1]. They found that, for certain values of the curvature, torsion and fluid flux, two counter-rotating cells can develop in the secondary flow in the cross-section, which could have important implications for the efficiency of particle separation.

Whilst the shape of the channel cross-section is one of the main factors that separator designers are able to control, previous work by Stokes *et al.* [21] and Arnold, Stokes, and Green [1] considered only rectangular channels, so as to simplify the governing equations. Here, we have relaxed this assumption so as to consider the effects of cross-sectional shape on the flow. This has, in turn, had a number of significant consequences not met in previous work. Firstly the coordinate system, and in particular the direction normal to the channel bottom, employed in Arnold, Stokes, and Green [1] was found to lead to complications in the case of non-rectangular channel cross-sections so that we have here formulated a general coordinate system with the direction normal to the channel bottom replaced by the vertical coordinate direction measured from the (arbitrary) channel bottom; see section II. Significant work was then required to express the Navier-Stokes equations in this general coordinate system and to obtain the thin-film approximation, assuming the fluid depth to be small in the vertical direction . Furthermore, the solution of the ODE for the fluid depth cannot be obtained analytically as in the rectangular channel case but must be solved numerically. Lastly we point out that, whereas for channels of rectangular cross-section the positions of the side walls are known and the (non-zero) depths of fluid at each wall are determined for a given flux, for channel cross-sections of arbitrary shape the fluid depth at either side can be zero, in which case the horizontal position(s) of the contact point(s) of the free surface with the channel bottom must be determined for a given flux. Thus there is an increased number of parameters in the problem which calls for a more complicated algorithm to handle all the various possibilities.

Although a consideration of channels of non-rectangular cross-section is new in the context of flow in helically-wound channels, for the case of a straight channel of arbitrary cross-sectional shape, the free surface flow problem has been studied by a number of authors, including Bowen and King [22], Holland, Duffy, and Wilson [23] and Wilson and Duffy [24,25]. Their work has considered additional effects, such as time-dependence, surface tension, and heat transfer which are neglected here. Neither surface tension or heat transfer are relevant to spiral particle separation in unheated channels with typical widths of half a metre or more while, at present, we seek steady-state solutions and leave time-dependence to future work. We anticipate that the presence of particles in the slurries transported in spiral separators will affect the flow but, in the present work, particle effects are also neglected to enable us to develop a basic understanding of the fluid motion. We note that Lee, Stokes, and Bertozzi [26] considered the flow of a monodisperse suspension in a helical channel, in the limiting case of small channel slope. We aim to consider particle effects in future work.

This paper is organised as follows. In section II we introduce the coordinate system and governing equations, apply a thin-film scaling, and present the solution method. In section III, we present and discuss results, before giving conclusions in section IV.

II. MATHEMATICAL MODEL

We consider free surface flow in a helically wound channel; for the purposes of illustration, a channel of parabolic cross-section is shown in figure 1. Here we extend previous work by allowing the cross-sectional shape to be arbitrary, although we require it to be shallow and independent of distance along the channel centreline. We study the steady state flow, ignoring inlet and outlet regions and assume that the flow is helically symmetric; that is, independent of distance along any helix of the same pitch and orientation as the channel centreline.

The governing equations of the flow are the steady Navier-Stokes equations,

$$\rho\left(\mathbf{v}\cdot\nabla\mathbf{v}\right)=-\nabla p+\nabla\cdot\left(\mu\mathcal{S}\right)-\rho g\hat{\mathbf{k}}, \tag{1}$$

where $\mathbf{v}$ is the velocity, ρ is the fluid density, p is the pressure, μ is viscosity, $\mathcal{S}$ is the rate-of-strain tensor and g is the acceleration due to gravity. The continuity equation,

$$\nabla\cdot\mathbf{v}=0. \tag{2}$$

We choose to use a coordinate system that permits a simple description of the flow geometry, as described below. We note similar systems have been used in Manoussaki and Chadwick [5], Lee, Stokes, and Bertozzi [26] and Arnold, Stokes, and Green [1] for rectangular channels with the bottom aligned horizontally in the radial direction. Here, for channels of arbitrary shape, we introduce a new term so that the channel bottom remains a coordinate surface.

ACCEPTED MANUSCRIPT

This manuscript was accepted by Phys. Fluids. Click here to see the version of record.

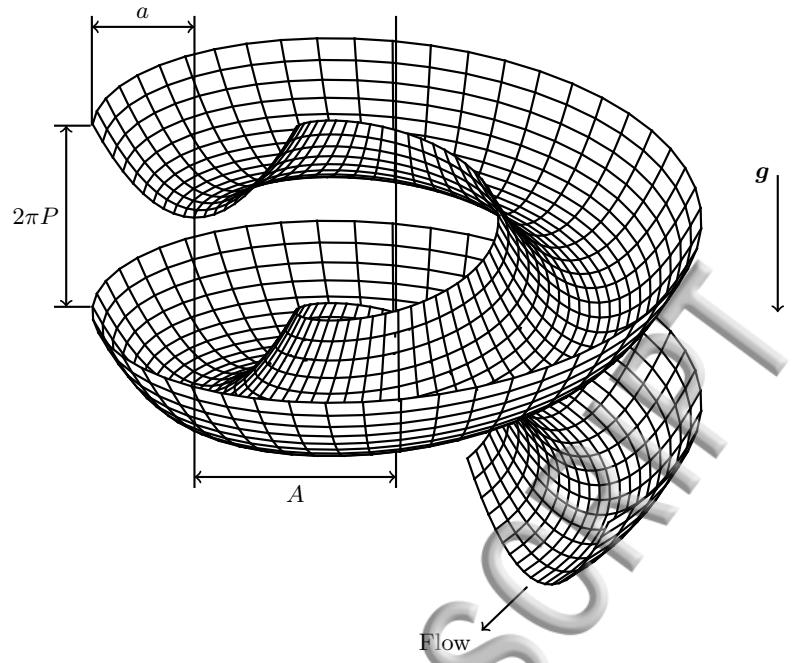

FIG. 1: A helically-wound channel with parabolic cross-section. The centreline is a helix of radius A and pitch $2\pi P$.

A. Coordinate system

We define a point in the fluid by its radius r (measured horizontally from the vertical axis around which the channel is wound), angle β about the vertical axis from a reference position, and vertical distance z from the channel bottom, as

$$\mathbf{x}(r,\beta,z) = r\cos(\beta)\hat{\mathbf{i}} + r\sin(\beta)\hat{\mathbf{j}} + (P\beta + H(r) + z)\hat{\mathbf{k}} \tag{3}$$

where $2\pi P$ is the pitch of the helix and $H(r)$ is the channel bottom profile. The coordinate system is shown in figure 2, together with a vertically-cut cross-section of the channel. For a channel with rectangular cross-section, $H(r) = 0$ and this coordinate system is equivalent to that used by Lee, Stokes, and Bertozzi [26] and Arnold, Stokes, and Green [1]. Since this is a non-orthogonal coordinate system, the techniques of tensor calculus must be used to write the Navier-Stokes equations. The details are similar to Lee, Stokes, and Bertozzi [26], however we choose not to introduce the coordinate direction normal to the channel bottom, as with an arbitrary cross-section it is simpler to visualise the vertical direction than the normal direction and use of the normal coordinate direction leads to non-uniqueness of coordinates for points in the fluid domain. **We omit the details of the derivation, but present the helically-symmetric (*i.e.* β-independent) form of the Navier-Stokes equations. After defining Φ as**

$$\Phi = 1 + \frac{P^2}{r^2} + H'(r)^2 \tag{4}$$

we can write the three components of the Navier-Stokes equations as, in the radial direction,

$$\begin{aligned}
&\rho\left(v^r\frac{\partial v^r}{\partial r} + v^z\frac{\partial v^r}{\partial z} - rv^\beta v^\beta\right)\\
&= -\frac{\partial p}{\partial r} + H'(r)\frac{\partial p}{\partial z} + \mu\left(\frac{\partial^2 v^r}{\partial r^2} + \frac{1}{r}\frac{\partial v^r}{\partial r} - \left[\frac{2}{r}H'(r) + 2H''(r)\right]\frac{\partial v^r}{\partial z}\right.\\
&\left. -3H'(r)\frac{\partial^2 v^r}{\partial z\partial r} + \Phi\frac{\partial^2 v^r}{\partial z^2} - H'(r)\frac{\partial^2 v^z}{\partial z^2} + \frac{2P}{r}\frac{\partial v^\beta}{\partial z} - \frac{1}{r^2}v^r\right),
\end{aligned} \tag{5}$$

ACCEPTED MANUSCRIPT

This manuscript was accepted by Phys. Fluids. Click here to see the version of record.

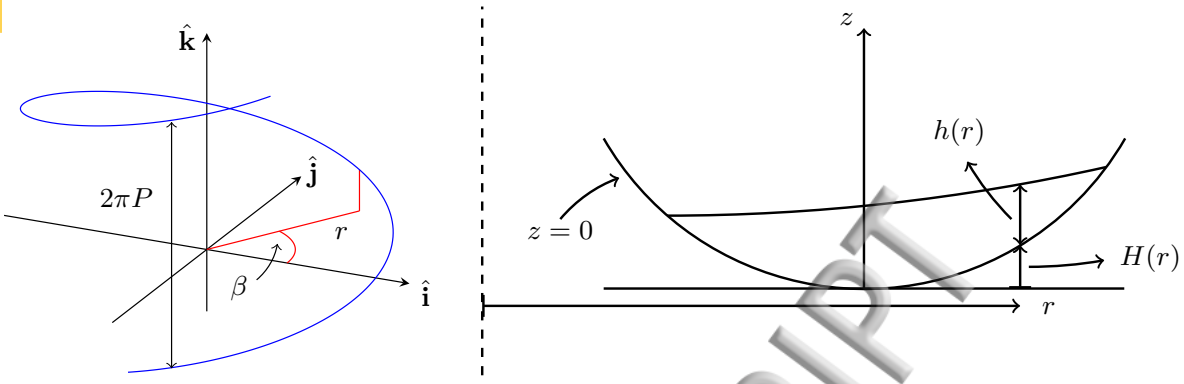

FIG. 2: The helical coordinate system. On the left is shown a helix with radius r and pitch $2\pi P$. On the right is a vertically-cut cross-section of a helical channel with a curved bottom.

in the axial direction,

$$\rho\left(v^r\frac{\partial v^\beta}{\partial r}+v^z\frac{\partial v^\beta}{\partial z}+\frac{2}{r}v^rv^\beta\right)$$
$$=\frac{P}{r^2}\frac{\partial p}{\partial z}+\mu\left(\frac{\partial^2 v^\beta}{\partial r^2}-\left[H''(r)+\frac{3}{r}H'(r)\right]\frac{\partial v^\beta}{\partial z}-2H'(r)\frac{\partial^2 v^\beta}{\partial z\partial r}+\Phi\frac{\partial^2 v^\beta}{\partial z^2}+\frac{3}{r}\frac{\partial v^\beta}{\partial r}-\frac{2P}{r^3}\frac{\partial v^r}{\partial z}\right), \tag{6}$$

and in the vertical direction,

$$\rho\left(v^r\frac{\partial v^z}{\partial r}+v^z\frac{\partial v^z}{\partial z}+rH'(r)v^\beta v^\beta+H''(r)v^rv^r-\frac{2P}{r}v^\beta v^r\right)$$
$$=H'(r)\frac{\partial p}{\partial r}-\Phi\frac{\partial p}{\partial z}+\mu\left(\left[2H''(r)-\frac{H'(r)}{r}\right]\frac{\partial v^r}{\partial r}-H'(r)\frac{\partial^2 v^r}{\partial r^2}+\left[H'''(r)+\frac{H''(r)}{r}+\frac{2H'(r)}{r^2}\right]v^r+\frac{\partial^2 v^z}{\partial r^2}\right.$$
$$\left.+\left[\frac{2P^2}{r^3}-2H''(r)H'(r)\right]\frac{\partial v^r}{\partial z}-\left[H''(r)+\frac{H'(r)}{r}\right]\frac{\partial v^z}{\partial z}-3H'(r)\frac{\partial^2 v^z}{\partial z\partial r}+\Phi\frac{\partial^2 v^z}{\partial z^2}+\frac{1}{r}\frac{\partial v^z}{\partial r}-\frac{2P}{r}\frac{\partial v^\beta}{\partial r}\right)-\rho g. \tag{7}$$

The continuity equation is,

$$\frac{\partial v^r}{\partial r}+\frac{\partial v^z}{\partial z}+\frac{1}{r}v^r=0. \tag{8}$$

B. Thin-film equations

The helically-symmetric steady Navier-Stokes equations, as shown in the previous section, are very complicated and some simplifications are necessary to facilitate analytic progress. The helical symmetry assumption means that the flow is independent of the distance along helices with the same pitch as the channel centreline, and our coordinate system allows us to impose this condition by making all quantities independent of β. Since the fluid depth in spiral separators is typically very small relative to the channel width, we use a thin-film approximation. Using a characteristic fluid depth $\bar{h}$ and the channel half-width a, $\delta=\bar{h}/a$ is a measure of the aspect ratio of the fluid. In the thin-film approximation, we assume $\delta\ll 1$. We nondimensionalise the governing equations using the channel half-width a, and axial velocity scale U, as follows (using hats to denote dimensionless variables and parameters)

$$r=a(\hat{A}+\hat{y}),\quad z=a\delta\hat{z}, \tag{9}$$

$$\mathbf{v}=(v,u,w)=\left(U\delta\hat{v},U\hat{u},U\delta^2\hat{w}\right), \tag{10}$$

ACCEPTED MANUSCRIPT

This manuscript was accepted by Phys. Fluids. Click here to see the version of record.

$$p = \frac{\mu U}{a\delta}\hat{p}, \quad H(r) = a\delta\hat{H}(\hat{y}). \tag{11}$$

The non-dimensional radius of the channel centreline $\hat{A}$, is given by $\hat{A} = A/a$, where A is the dimensional radius of the channel centreline. The new variable $\hat{y}$ is a dimensionless radial position, measured from the designated centreline of the channel. Explicit definitions of U and δ in terms of the physical parameters of the problem will be given later **in equation** (32).

We next define some notation that will help simplify the equations. The channel centreline has dimensionless radius $\hat{A}$, and we define the nondimensional curvature-like parameter $\epsilon = 1/\hat{A}$, and the dimensionless pitch, $\hat{P} = P/a$. The slope of the channel centreline, λ, is given by $\lambda = \hat{P}/\hat{A}$. The **dimensionless** torsion, $\hat{\tau}$, and curvature, $\hat{\kappa}$, of the channel at $\hat{y}$ are given by

$$\hat{\kappa}(\hat{y}) = \frac{\epsilon}{(1+\epsilon\hat{y})\Upsilon(\hat{y})}, \quad \hat{\tau}(\hat{y}) = \Lambda(\hat{y})\hat{\kappa}(\hat{y}), \tag{12}$$

where

$$\Lambda(\hat{y}) = \frac{\lambda}{1+\epsilon\hat{y}}, \tag{13}$$

is the slope of the channel bottom at $\hat{y}$, and

$$\Upsilon(\hat{y}) = 1 + \Lambda(\hat{y})^2. \tag{14}$$

After nondimensionalising and taking the thin-film limit, $\delta \to 0$, the leading order governing equations are (dropping hats on dimensionless variables),

$$\frac{\partial^2 v}{\partial z^2} = -\frac{\epsilon \mathrm{Re}}{(1+\epsilon y)\Upsilon^2}u^2 + \frac{1}{\Upsilon}\frac{\partial p}{\partial y} - \frac{2\epsilon\Lambda}{(1+\epsilon y)\Upsilon^{3/2}}\frac{\partial u}{\partial z} - \frac{1}{\Upsilon}\frac{\partial p}{\partial z}\frac{\mathrm{d}H}{\mathrm{d}y}, \tag{15a}$$

$$\frac{\partial^2 u}{\partial z^2} = -\frac{\Lambda}{\sqrt{\Upsilon}}\frac{\partial p}{\partial z}, \tag{15b}$$

$$\frac{\partial p}{\partial z} = -\frac{\mathrm{Re}}{\mathrm{Fr}^2}\frac{1}{\Upsilon}, \tag{15c}$$

and

$$\frac{\partial v}{\partial y} + \frac{\epsilon v}{1+\epsilon y} + \frac{\partial w}{\partial z} = 0, \tag{16}$$

where we have defined the Reynolds number, Re, and Froude number, Fr, as

$$\mathrm{Re} = \frac{\rho U a\delta}{\mu}, \quad \mathrm{Fr} = \frac{U}{\sqrt{ga\delta}}. \tag{17}$$

The boundary conditions are no-slip on the channel bottom,

$$u = v = w = 0 \text{ on } z = 0, \tag{18}$$

no stress on the free-surface,

$$p = \frac{\partial u}{\partial z} = \frac{\partial v}{\partial z} = 0 \text{ on } z = h(y), \tag{19}$$

and the kinematic condition at the free-surface,

$$v\frac{\mathrm{d}h}{\mathrm{d}y} = w \text{ on } z = h(y). \tag{20}$$

This model for thin-film flow in a shallow helically-wound channel of arbitrary cross-section has a form that is surprisingly similar to that given in Arnold, Stokes, and Green [1] for a channel of rectangular cross-section and which uses a different coordinate system. This was not anticipated but allows us to proceed with analytic solution of the model in a similar manner up to solving for the free surface which must now be done numerically and allow for determining the horizontal positions of the points of contact of the free surface with the channel bottom.

As discussed in Stokes *et al.* [21], Lee, Stokes, and Bertozzi [26] and Arnold, Stokes, and Green [1], we cannot impose no-slip conditions at vertical channel walls, should they exist. This is a result of the thin-film scaling, and we would anticipate the presence of thin boundary layers near vertical walls, which are not captured in our leading order equations, and which do not have a significant effect on the flow away from the vertical walls. We will discuss this further in section III A.

ACCEPTED MANUSCRIPT

This manuscript was accepted by Phys. Fluids. Click here to see the version of record.

C. Solution of the thin-film equations

The leading order thin-film Navier-Stokes equations (15a)–(15c) can be solved by integrating, subject to boundary conditions, to give

$$p = -\frac{\mathrm{Re}}{\mathrm{Fr}^2}\frac{(z-h)}{\Upsilon}, \tag{21}$$

$$u = \frac{\mathrm{Re}}{\mathrm{Fr}^2}\frac{\Lambda}{\Upsilon^{3/2}}\frac{z(z-2h)}{2}, \tag{22}$$

$$\begin{aligned} v = &-\frac{\mathrm{Re}^3}{\mathrm{Fr}^4}\frac{\epsilon\Lambda^2}{(1+\epsilon y)\Upsilon^5}\frac{z(z^5-6hz^4+10h^2z^3-16h^5)}{120} \\ &-2\frac{\mathrm{Re}}{\mathrm{Fr}^2}\frac{\epsilon\Lambda^2}{(1+\epsilon y)\Upsilon^3}\frac{(z-h)^3+h^3}{3}+\frac{\mathrm{Re}}{\mathrm{Fr}^2}\frac{1}{\Upsilon^2}\frac{\mathrm{d}}{\mathrm{d}y}(H+h)\frac{z(z-2h)}{2}. \end{aligned} \tag{23}$$

By integrating the continuity equation (16), changing the order of differentiation and integration, and requiring that there is no net flux into or out of the fluid domain, we obtain

$$\int_0^{h(y)} v\,\mathrm{d}z = 0 \tag{24}$$

which can be evaluated and rearranged to give a differential equation for the fluid depth $h(y)$,

$$\frac{\mathrm{d}h}{\mathrm{d}y} = \frac{6}{35}\frac{\mathrm{Re}^2}{\mathrm{Fr}^2}\frac{\epsilon\Lambda^2}{(1+\epsilon y)\Upsilon^3}h^4 - \frac{3}{2}\frac{\epsilon\Lambda^2}{(1+\epsilon y)\Upsilon}h - \frac{\mathrm{d}H}{\mathrm{d}y}. \tag{25}$$

This is a Chini differential equation, and in general has no analytic solution and must be solved numerically **(we use the `ode45` function provide by Matlab)**. In the special case of a rectangular channel, where $H(y) = 0$, the free-surface equation does have an analytic solution[1], which can be found using the substitution $\xi = h^{-3}$.

Substituting (25) into (23) gives a simpler form for the radial velocity component,

$$v = -\frac{\mathrm{Re}^3}{\mathrm{Fr}^4}\frac{\epsilon\Lambda^2}{(1+\epsilon y)\Upsilon^5}\frac{7z^6-42hz^5+70h^2z^4-72h^4z^2+32h^5z}{840} - \frac{\mathrm{Re}}{\mathrm{Fr}^2}\frac{\epsilon\Lambda^2}{(1+\epsilon y)\Upsilon^3}\frac{8z^3-15hz^2+6h^2z}{12}. \tag{26}$$

We note that due to the very large denominator in the first term, v is approximately zero when the second term is zero, which occurs when $z = (15-\sqrt{33})h/16 \approx 0.5785h$. Thus the secondary flow is vertical at roughly 58% of the fluid depth.

A streamfunction, ψ, for the secondary flow (the radial and vertical components of $\mathbf{v}$), is defined by

$$\frac{\partial\psi}{\partial z} = (1+\epsilon y)v, \quad \frac{\partial\psi}{\partial y} = -(1+\epsilon y)w, \tag{27}$$

and we specify $\psi = 0$ on the channel bottom $z = 0$ and the free surface $z = h(y)$, which together form a closed streamline.

Integrating the first equation in (27), we obtain the streamfunction as

$$\psi = -\frac{\mathrm{Re}^3}{\mathrm{Fr}^4}\frac{\epsilon\Lambda^2}{\Upsilon^5}\frac{z^2(z-h)(z-2h)^2(z^2-2hz-4h^2)}{840} - \frac{\mathrm{Re}}{\mathrm{Fr}^2}\frac{\epsilon\Lambda^2}{\Upsilon^3}\frac{z^2(z-h)(2z-3h)}{12}, \tag{28}$$

which can be substituted into the second equation in (27) to give the vertical velocity w.

The fluid flux down the channel, Q, is scaled by $\delta a^2 U$ and is given by

$$\begin{aligned} Q =& -\int_{y_l}^{y_r}\int_0^{h(y)} u(z,y)\,\mathrm{d}z\,\mathrm{d}y \\ =& \frac{1}{3}\frac{\mathrm{Re}}{\mathrm{Fr}^2}\int_{y_l}^{y_r}\frac{\Lambda h^3}{\Upsilon^{3/2}}\,\mathrm{d}y. \end{aligned} \tag{29}$$

ACCEPTED MANUSCRIPT

This manuscript was accepted by Phys. Fluids. Click here to see the version of record.

where $y = y_l$ and $y = y_r$ are the left and right contact points of the free-surface with the channel wall(s) or channel bottom. The minus sign appears because the positive axial direction points in the upstream direction, thus u is negative. The cross-sectional area of the fluid, scaled by δa^2, is given by

$$\Omega = \int_{y_l}^{y_r} h \, \mathrm{d}y. \tag{30}$$

These integrals cannot be computed exactly (even in the rectangular channel case) and must be determined numerically.

In order to examine solutions, we must prescribe the velocity scale U, and thin-film parameter δ. Following Arnold, Stokes, and Green [1], we require that the coefficient on the $z(z-2h)/2$ term in (22), and the coefficient on the h^4 term in (25) both have unit value at $y = 0$ to give non-trivial free-surface shapes and flow solutions. These scalings give,

$$\frac{\mathrm{Re}}{\mathrm{Fr}^2}\frac{\lambda}{(1+\lambda^2)^{3/2}} = 1 \quad \text{and} \quad \frac{6}{35}\mathrm{Re}\frac{\epsilon\lambda}{(1+\lambda^2)^{3/2}} = 1, \tag{31}$$

which can be rearranged, using the definitions of the Reynolds and Froude numbers as given previously, to give expressions for the velocity and film-thickness scales U and δ in terms of the geometric and fluid parameters, as

$$U = \left[\left(\frac{35}{6}\right)^2 \frac{1+\lambda^2}{\epsilon^2\lambda}\frac{g\mu}{\rho}\right]^{1/3} \quad \text{and} \quad \delta = \frac{1}{a}\left[\frac{35}{6}\frac{(1+\lambda^2)^3}{\epsilon\lambda^2}\frac{\mu^2}{g\rho^2}\right]^{1/3}. \tag{32}$$

The thin-film assumption requires $\delta \ll 1$, and using typical values for a channel of half-width $a = 0.1$ m carrying water ($\rho = 10^3$ kg m^{-3}, $\mu = 10^{-3}$ kg m^{-3}), we require

$$\frac{(1+\lambda^2)^3}{\epsilon\lambda^2} \ll 10^{10}, \tag{33}$$

which is always true for channels of physical interest, and fails only for very flat ($\lambda \to 0$), gently curving ($\epsilon \to 0$), or steeply sloping ($\lambda \to \infty$) channels.

D. Implementation

In Arnold, Stokes, and Green [1] in which $H(y) = 0$, $y_l = -1$ and $y_r = 1$, once the radius and pitch of the channel centreline were defined (using ϵ and λ), **the only parameters left were h_l, the fluid depth at the left channel wall y_l, h_r, the fluid depth at the right channel wall y_r, as well as Q, the fluid flux down the channel**. Specifying one of these three parameters determined the other two. The flux was chosen as the most physically relevant parameter to specify. For a channel with arbitrary cross section, we must add y_l and y_r to the parameters of the problem, which now number five, $\{y_l, y_r, h_l, h_r, Q\}$. Three of these must be specified, which determine the other two. It is possible to have zero or non-zero fluid depth at either edge of the fluid domain, leading to several different cases. We note that $h_l \geq 0$ and $h_r \geq 0$, with non-zero values meaning there is a vertical channel wall at the corresponding y_l and/or y_r. For any channel shape, we can again specify the flux, and any two of $\{y_l, y_r, h_l, h_r\}$ depending on the problem of interest. The process to obtain a solution can be described in the following steps:

1. Choose the channel cross-sectional shape $H(y)$, geometric parameters ϵ and λ, and the flux Q;
2. Choose values of two of the parameters from $\{y_l, y_r, h_l, h_r\}$;
3. Use a root-finding algorithm and the free-surface equation to determine the last two unknown paramters.

We sometimes choose not to prescribe a flux but simply specify three of the four geometrical parameters and directly calculate the fourth and the resultant flux.

III. RESULTS

We now investigate solutions of the thin-film equations. Arnold, Stokes, and Green [1] examined rectangular channels and drew several conclusions about the effects of ϵ, λ and flux on the resultant flow. In section III A we show some results from channels with rectangular cross-section, and by comparing with a nearly-rectangular channel (with no

ACCEPTED MANUSCRIPT

This manuscript was accepted by Phys. Fluids. Click here to see the version of record.

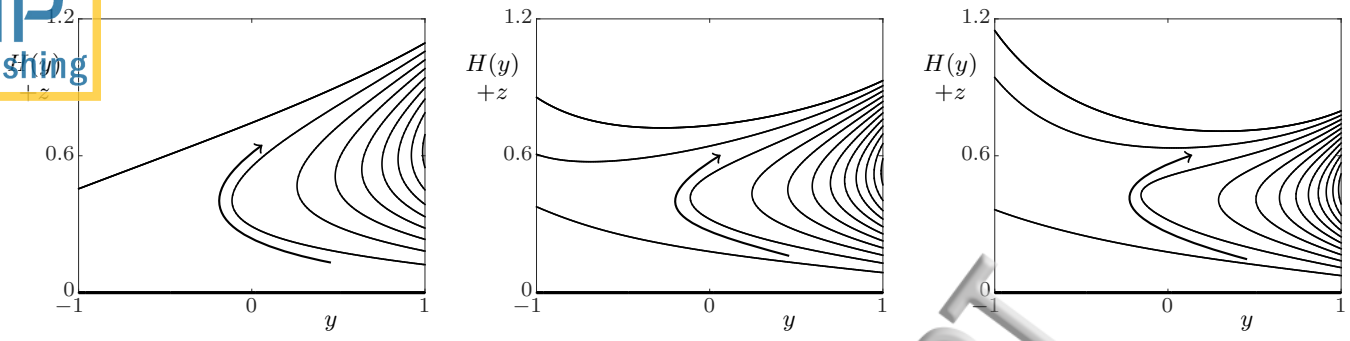

(a) $\lambda = 0.1$ (b) $\lambda = 0.8$ (c) $\lambda = 1.5$

FIG. 3: Rectangular channel with $\epsilon = 0.5$, $Q = 0.1$, and varying λ. Note the channel bottom is the bottom of the figure, $z = 0$. Arrows indicate the direction of the secondary flow.

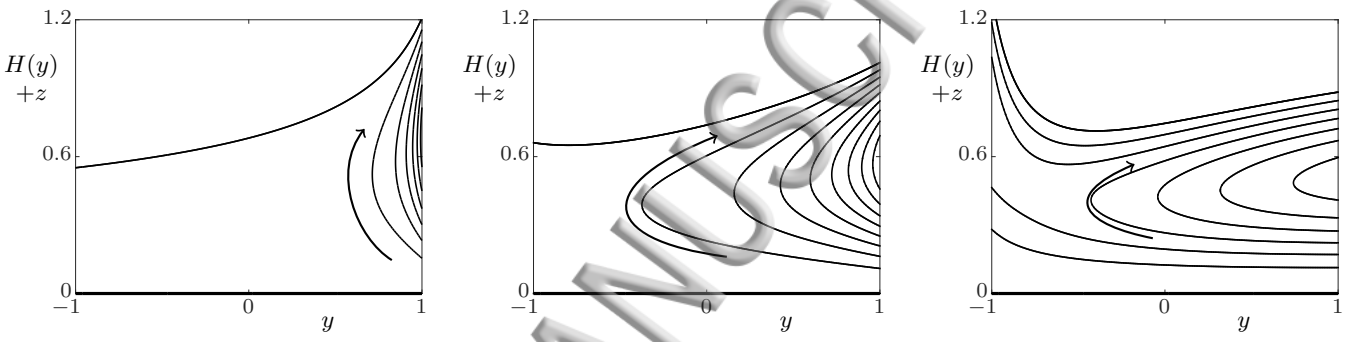

(a) $\epsilon = 0.1$ (b) $\epsilon = 0.5$ (c) $\epsilon = 0.8$

FIG. 4: Rectangular channel with $\lambda = 0.5$, $Q = 0.1$, and varying ϵ. Note the channel bottom is the bottom of the figure, $z = 0$. Arrows indicate the direction of the secondary flow.

slip on the entire channel surface), demonstrate the small inaccuracy resulting from being unable to impose the no-slip boundary condition on vertical channel walls. We then move on to investigate non-rectangular channels more generally. In section III B we consider channels with sloping bottoms, which for small slopes are very similar to rectangular channels. We also consider so-called tick shaped channels, with larger slope and a vertical wall on only one side of the channel. In section III C we look at some channels with curved bottoms.

A. Rectangular and nearly-rectangular channels

Channels with rectangular cross-section were extensively studied in Arnold, Stokes, and Green [1], and we briefly recapitulate some of those results to provide a point of comparison with channels of other shapes, noting that the vertical coordinate direction used here is different to the normal direction used in that paper. In figures 3 and 4, we plot free-surface profiles and streamfunctions, holding all parameters constant with the exception of either λ or ϵ. The flow always moves from the inside to the outside channel wall at the free-surface, and from the outside to the inside wall near the channel bottom. The secondary flow is generally clockwise rotation around some point, but can break into separate clockwise rotating cells[1]. Increasing either λ or ϵ, which increases the slope $\Lambda(y)$ near the inside channel wall, tends to increase the fluid depth at the inside channel wall, whilst decreasing these parameters tends to increase the fluid depth at the outside channel wall. In Arnold, Stokes, and Green [1] this behaviour was explained by the competition of two effects, gravitational force pushing fluid to the steepest part of the channel (the inside wall), and inertial forces pushing fluid to the outside channel wall.

We now consider the impact of our inability to apply the no-slip boundary condition on vertical channel walls due to the thin-film scaling. In section II B, it was claimed that in practice we would expect thin boundary layers near the channel walls, which would not have a significant impact on the results. Stokes *et al.* [21] compared numerical simulations

ACCEPTED MANUSCRIPT

This manuscript was accepted by Phys. Fluids. Click here to see the version of record.

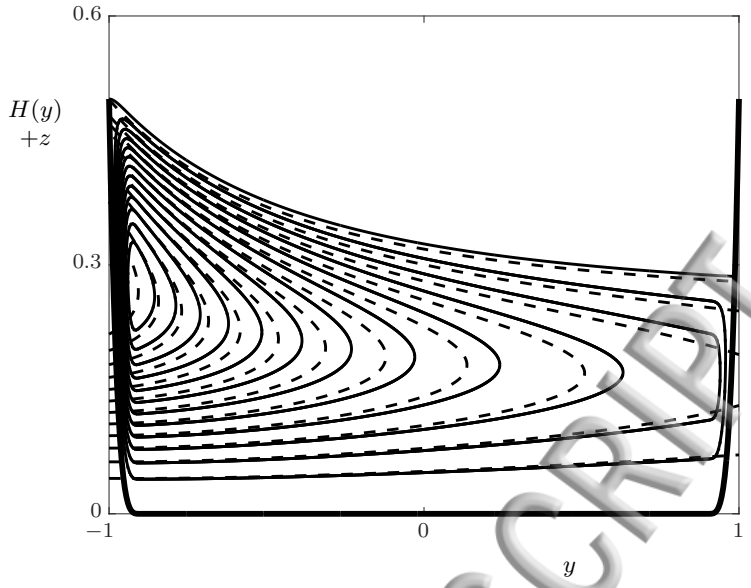

FIG. 5: Rectangular and nearly-rectangular channel, $\epsilon = 0.5$, $\lambda = 0.7$. Dashed lines correspond to the rectangular channel, and solid lines to the nearly-rectangular approximation. Contour levels are the same in both cases.

for a rectangular channel with thin-film results, valid in the limits of small ϵ and λ, which showed excellent agreement away from the channel side walls, and boundary layers near them. We here show the effect of boundary layers by comparing results for a rectangular channel with results for a nearly-rectangular channel, with no discontinuities in the slope of the channel wall. We construct such a channel with side walls using quartic polynomials that smoothly join to the flat channel bottom, as

$$H(y) = \begin{cases} k\dfrac{(y+y^*)^4}{(1-y^*)^4}, & -1 \le y \le -y^* \\ 0, & -y^* < y < y^* \\ k\dfrac{(y-y^*)^4}{(1-y^*)^4}, & y^* \le y \le 1 \end{cases}, \tag{34}$$

where k is the height at the edges of the channel, $y = \pm 1$, and $\pm y^*$ are the positions at which the curved side walls meet the horizontal channel bottom so that y^* determines how close the channel cross-section is to rectangular. The secondary flow for a channel with $k = 0.5$ and $y^* = 0.9$ is shown in figure 5, along with that for a rectangular channel with vertical walls. We see very good agreement in the interior of the channel, which deteriorates near the edges, as expected. The most notable difference is the anticipated existence of boundary layers near the side walls of the nearly-rectangular channel which are not seen for the rectangular channel. The free-surface profiles are very similar, but for the same flux that of the rectangular channel is slightly lower than the nearly-rectangular channel because of the extra cross-sectional area gained with vertical side walls. The correspondence between the two solutions justifies the study of channels with vertical walls using the thin-film approximation, with the error introduced by the lack of the no-slip boundary condition on the side walls being a local effect that does not change the qualitative behaviour of the solution.

B. Channels with a sloping bottom

Next we consider channels with a bottom of constant slope k, i.e. $H(y) = ky$. Figure 6 shows solutions for three different slopes k, each with the same ϵ, λ and Q. There is little difference in the free-surface, but there is a significant effect on slope of the secondary flow. Figure 6(a) shows the secondary flow for a channel with negative slope, which has broken up into two rotating cells. For $k = 0$ and $k = 0.05$, the secondary flow does not exhibit multiple rotating cells. For channels with $\epsilon = 0.5$, $\lambda = 0.75$, and $Q = 0.1$, multiple rotating cells are seen for channel slopes less than roughly $k = -0.02$. Thus, the break-up into multiple rotating cells, remarked upon in Arnold, Stokes, and Green [1], is

ACCEPTED MANUSCRIPT

This manuscript was accepted by Phys. Fluids. Click here to see the version of record.

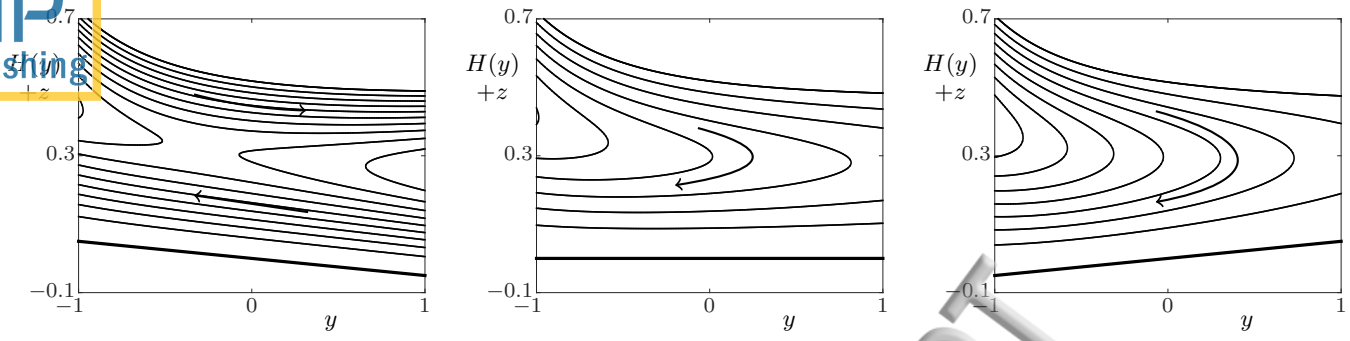

(a) $k = -0.05$ (b) $k = 0$ (c) $k = 0.05$

FIG. 6: Sloping channels, $H(y) = ky$, for varying k, with $\epsilon = 0.5$, $\lambda = 0.75$ and $Q = 0.1$. Arrows indicate the direction of the secondary flow.

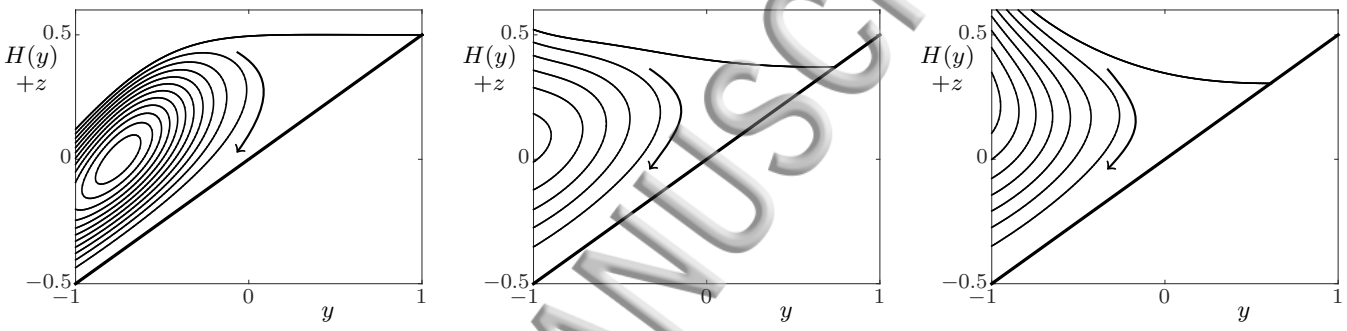

(a) $\lambda = 0.2$ (b) $\lambda = 0.8$ (c) $\lambda = 1.4$

FIG. 7: Tick shaped channel $H(y) = y/2$, varying λ, with $\epsilon = 0.5$ and $Q = 0.15$. Arrows indicate the direction of the secondary flow.

not limited to rectangular channels, and is influenced by the channel bottom slope. The free surface profiles for the three different channel slopes are very similar, despite the significant changes in the secondary flow. The sensitivity of the free surface profile will be further discussed in section III C.

If the free surface contacts the bottom of the channel at one end and a vertical channel wall at the other we have what we term a tick-shaped channel. We have two cases, a channel with positive slope and the vertical wall at the inside of the channel, or a channel with negative slope and a vertical wall at the outside of the channel. The main difference from the sloping channel case is that we specify $y_l = -1$ and $h_r = 0$ or $y_r = 1$ and $h_l = 0$ in addition to the flux, and must determine h_l and y_r, or h_r and y_l, respectively. In figure 7 we show the effect of changing the down-channel slope (λ) of the channel centreline on the flows in tick shaped channels defined by $H(y) = y/2$ and with $\epsilon = 0.5$ and $Q = 0.15$. We see that as the slope λ increases, the fluid tends to move towards the inner channel wall, and the outer contact point also moves inwards. The same behaviour is observed when ϵ is increased (results not shown). This behaviour is qualitatively similar to the rectangular channel case, with a competition between inertial and gravitational effects. Figure 8 shows the case of a channel bottom shape with negative slope, $H(y) = -y/2$. As λ increases, we see the inner contact point moving inwards, and the outside fluid depth decreasing. Although not as dramatic as for the upwards sloping tick-shaped channel, the same behaviour is again seen; increasing the slope tends to push fluid to the inside of the channel.

In the limiting case of a gently curving and sloping channel ($\epsilon \to 0$ and $\lambda \to 0$) with $H(y) = ky$, the free surface equation (25) can be written as,

$$\frac{\mathrm{d}h}{\mathrm{d}y} = h^4 - k. \tag{35}$$

For a channel bottom profile with positive slope, $k > 0$, this equation has an exact implicit solution. Defining

ACCEPTED MANUSCRIPT

This manuscript was accepted by Phys. Fluids. Click here to see the version of record.

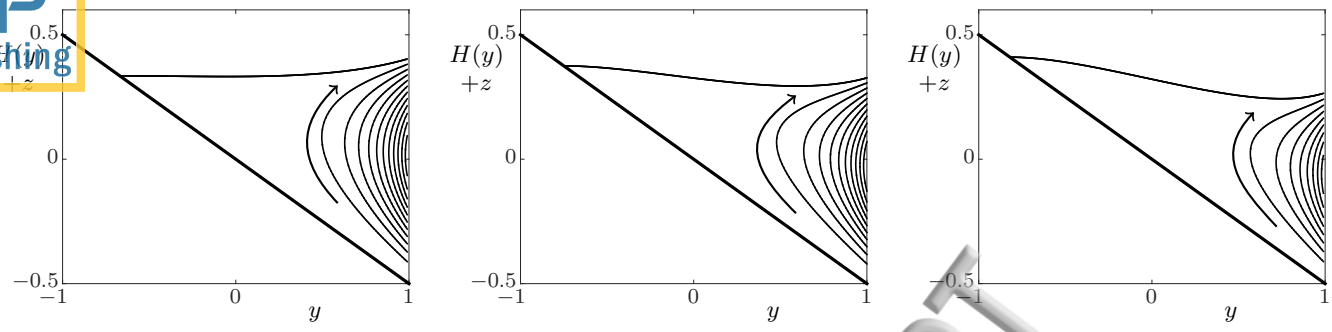

(a) $\lambda = 0.2$ (b) $\lambda = 0.8$ (c) $\lambda = 1.4$

FIG. 8: Tick shaped channel $H(y) = -y/2$, varying λ, with $\epsilon = 0.5$ and $Q = 0.07$. Arrows indicate the direction of the secondary flow.

$\chi = |k|^{1/4}$, we obtain

$$y - y_a = \frac{1}{4\chi^3} \log\left(\frac{\chi - h}{\chi + h}\right) - \frac{1}{2\chi^3} \arctan\left(\frac{h}{\chi}\right), \tag{36}$$

where y_a is the point where the free surface meets the channel bottom. For downwards sloping channels, with $k < 0$, the solution is more complicated,

$$y - y_a = \frac{1}{4\sqrt{2}\chi^3} \log\left(\frac{\chi^2 + \sqrt{2}\chi h + h^2}{\chi^2 - \sqrt{2}\chi h + h^2}\right) + \frac{1}{2\sqrt{2}\chi^3} \arctan\left(\frac{\sqrt{2}\chi h}{\chi^2 - h^2}\right). \tag{37}$$

Figure 9 shows a comparison between these implicit solutions and numerical solutions to the full free surface equation (25). Very good agreement is seen, even with these relatively large values of ϵ and λ.

The solutions presented above apply to channels with $k > 0$ and a vertical wall at the inside of the channel, or to channels with $k < 0$ and a vertical wall at the outside of the channel. Other options at first seem possible, namely, $k > 0$ and an outside vertical wall and $k < 0$ and an inside vertical wall. However, no solution exists for these latter cases for the following reason. If the fluid meets the channel bottom, its depth $h(y)$ must reach zero. Then, taking $h(y) = 0$ and rearranging the free-surface differential equation (25) gives

$$\frac{\mathrm{d}}{\mathrm{d}y}(h + H) = 0, \tag{38}$$

and so the free-surface must be horizontal when it contacts the channel bottom. This means that the fluid can meet the channel bottom at the outside of the channel if $H'(y) > 0$ there, and at the inside of the channel if $H'(y) < 0$ there. For tick-shaped channels, these restrictions on the sign of $H'(y)$ near the free-surface contact point are only satisfied in the two types of channels with solutions (36) and (37). In the cases where no solution exists, the channel would not be able to contain the fluid, which would pour out.

C. Channels with a curved bottom

We now consider channels with curved bottoms. Whilst there are many choices, we will first consider a simple parabolic channel $H(y) = 0.5y^2$. In figure 10 we present plots for this channel for fixed $\epsilon = 0.5$, $Q = 0.015$ and three different values of the down-channel slope of the channel centreline λ. We first note that since there are no vertical channel walls in this case, the no-slip boundary condition is satisfied along the whole channel bottom, and with $h_l = h_r = 0$, we must determine the parameters y_l and y_r for given ϵ, λ and Q. In figure 10 we see the change of y_l and y_r with λ for our chosen values of Q and ϵ. As for other channel shapes, we see that increasing λ tends to push the fluid to the inside of the channel, which also occurs when ϵ is increased (not shown). Decreasing ϵ or λ, or increasing the flux, causes the fluid to move further to the outside of the channel.

In section III B, it was noted that the secondary flow could be very sensitive to channel shape, but the free-surface was relatively less sensitive. We now show this for differently-shaped channels. In figure 11 two channels are shown,

ACCEPTED MANUSCRIPT

This manuscript was accepted by Phys. Fluids. Click here to see the version of record.

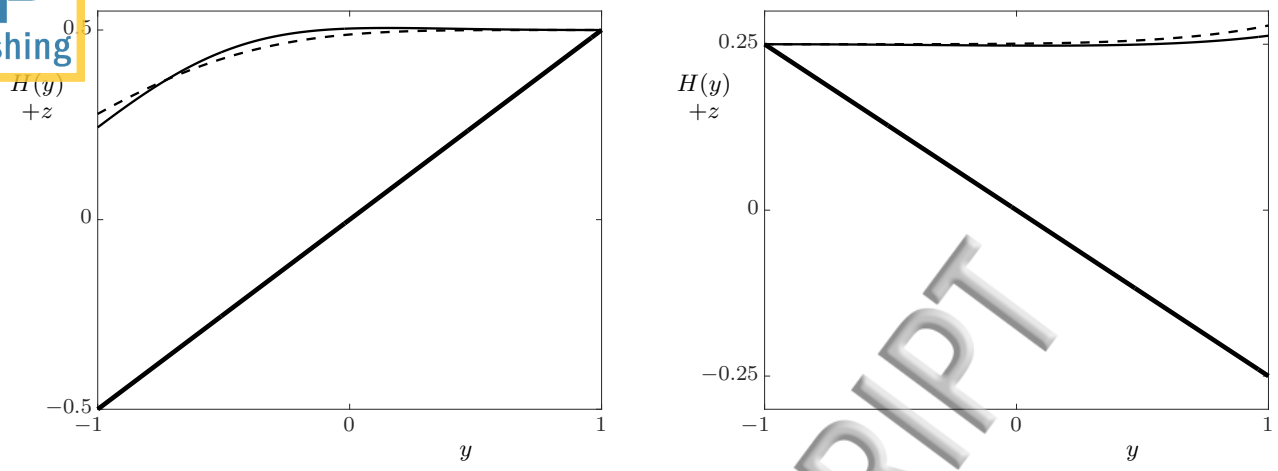

(a) $H(y) = y/2$, $\epsilon = 0.4$, $\lambda = 0.4$, and $Q \approx 0.125$. (b) $H(y) = -y/4$, $\epsilon = 0.1$, $\lambda = 0.4$, and $Q \approx 0.021$.

FIG. 9: Upwards and downwards sloping tick-shaped channels. The dashed line represents the analytic solution, and the solid line represents the numerical solution. Note the different parameters and ordinate scales in each figure. In both figures, $y_l = -1$ and $y_r = 1$ are specified.

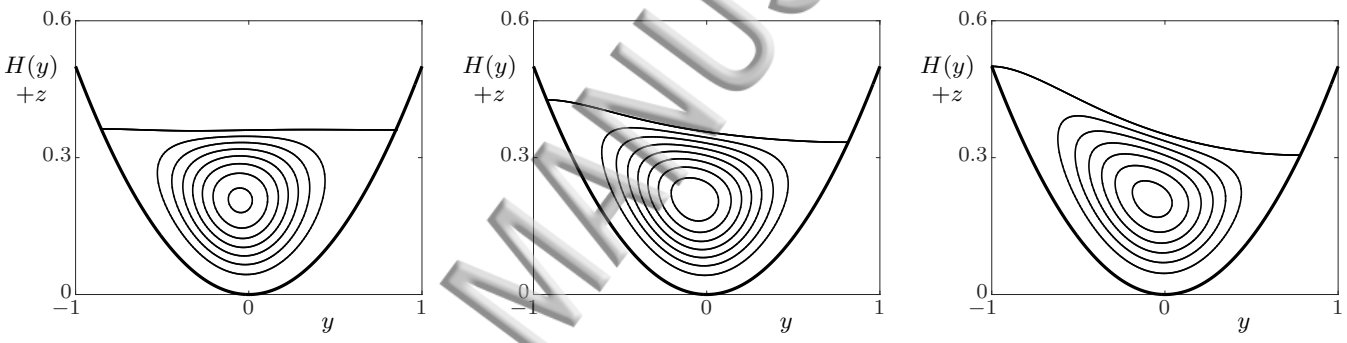

(a) $\lambda = 0.2$ (b) $\lambda = 0.6$ (c) $\lambda = 1$

FIG. 10: Parabolic channels with $\epsilon = 0.5$, $Q = 0.015$, and varying λ. Flow is clockwise around streamlines.

one with one bump in the bottom and one with two bumps. Both solutions have the same centreline radius and pitch, and the same flux. The channel bottom shape has a clear effect on the secondary flow, splitting it into multiple independent rotating cells, one more than the number of bumps. Looking at the streamlines that pass through the saddle points (which are stagnation points of the secondary flow) we see in figure 11(a) that the two cells are surrounded by a circulating flow in the region between the cells and the flow-domain boundaries, while in figure 11(b) there are two surrounding circulating flows, one around the inner and central cells and another around all three cells. The free-surface profiles, however, remain remarkably similar. The filled circles represent the centres (found using the 58% depth approximation found in section II C) of the rotating cells, and the crosses represent saddle points of the streamfunction. At both the filled circles and crosses, the secondary flow velocity is zero, and there is only an axial component of the fluid velocity.

To further investigate the sensitivity of the secondary flow to the channel shape, we consider a rectangular channel with a small bump in the channel bottom. The results for a channel with a growing bump are shown in figure 12. In these plots, the flux $Q = 1$, $y_l = -1$, and $y_r = 1$. We see that the free-surface profile is again fairly similar across the three bump heights, but there is a break up of the single rotating cell seen in figure 12(a), into two rotating cells inside a larger rotating cell even when the height of the bump is small, at roughly 5% of the depth of the fluid. As in figure 11, the filled circles are the centres of local rotating cells of fluid, although the cells are far less pronounced in these latter cases. In figure 13, we repeat the experiment using a parabolic channel with a narrow Gaussian bump and find again that the flow separates into multiple rotating cells even for a small bump height of 0.05, roughly 10% of the fluid depth. For the larger bump with height 0.1, the separate rotating cells become quite large, and a significant

ACCEPTED MANUSCRIPT

This manuscript was accepted by Phys. Fluids. Click here to see the version of record.

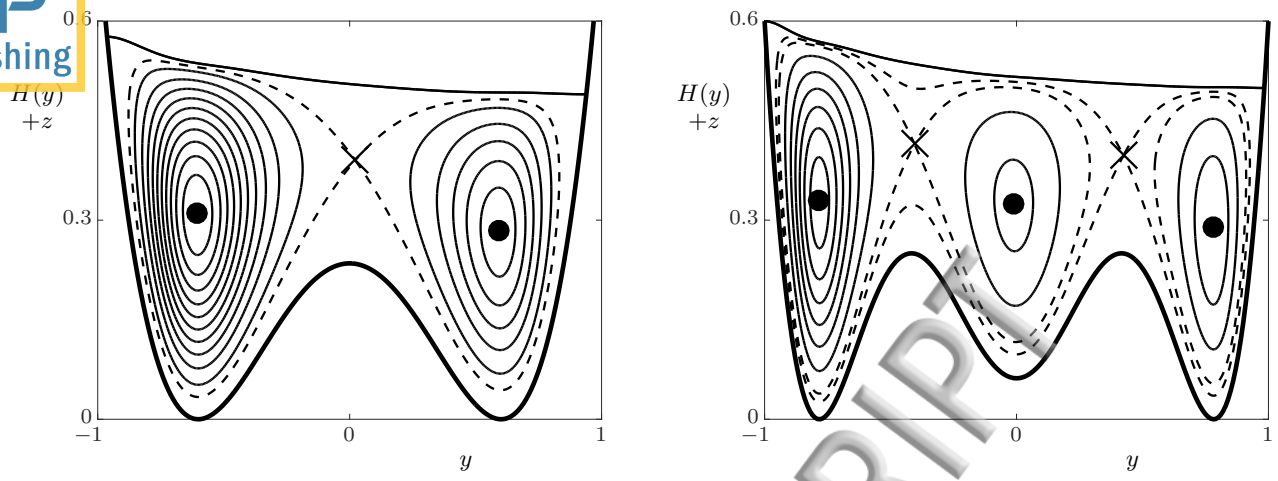

(a) One bump (b) Two bumps

FIG. 11: Bumpy channels, with $\epsilon = \lambda = 0.6$ and $Q \approx 0.042$. Filled circles represent a local maximum of the streamfunction and centre of a clockwise rotating cell, and crosses are saddle points. Dashed curves represent streamlines passing through saddle points which are also stagnation points of the secondary flow.

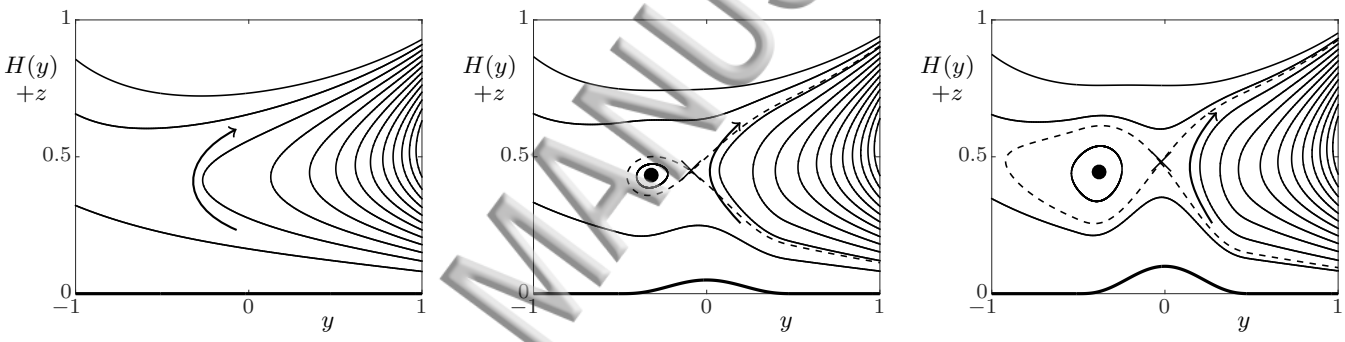

(a) No bump (b) Bump height 0.05 (c) Bump height 0.10

FIG. 12: Channels with a growing bump in the bottom, $\epsilon = 0.5$, $\lambda = 0.8$, and $Q = 1$. Filled circles represent a local maximum of the streamfunction and centre of a clockwise rotating cell, and crosses are saddle points. Dashed curves represent streamlines passing through saddle points.

proportion of the cross-sectional flow domain is taken up by these structures.

The breakup into multiple rotating cells is of interest in part due to its potential implications on particle separation efficiency in spiral separators. We hypothesise that having separate rotating cells could inhibit particle movement across the width of the channel. Whilst the break-up into multiple rotating cells can occur in rectangular channels due to the balance of gravitational and inertial effects, it is more readily seen as a result of the channel bottom shape.

IV. CONCLUSION

We have considered helically-symmetric thin-film flow in helical channels with arbitrary cross-sections. Using a helicoidal body-fitted coordinate system we obtained a system of equations that can be solved to give a simple differential equation for the free surface shape requiring numerical solution. In the special case of small channel centreline torsion and curvature, we obtained analytic solutions for so-called 'tick-shaped' channels.

The influence of the slope (λ) and radius ($1/\epsilon$) of the channel centreline on the competition between gravity and inertia and, hence, on the free surface shape and transverse flow, were studied extensively for rectangular channels in Arnold, Stokes, and Green[1]. We have observed the same qualitative behaviours in channels of arbitrary shape. The

ACCEPTED MANUSCRIPT

This manuscript was accepted by Phys. Fluids. Click here to see the version of record.

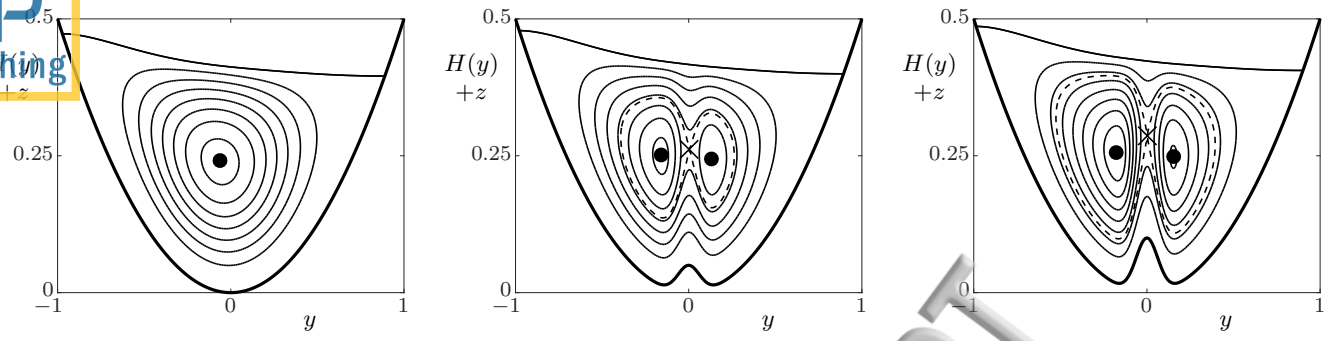

(a) No bump (b) Bump height 0.05 (c) Bump height 0.10

FIG. 13: Parabolic channels with a growing Gaussian bump in the bottom, $\epsilon = 0.5$, $\lambda = 0.5$, and $Q \approx 0.02$. Filled circles represent a local maximum of the streamfunction and centre of a clockwise rotating cell, and crosses are saddle points. Dashed curves show streamlines passing through saddle points.

downwards slope of the channel bottom is greater nearer to the vertical axis about which the channel is wound and this slope increases with both λ and ϵ. When the downward slope on the inside of the channel becomes sufficiently large gravity dominates and there is a build up of fluid there, while for smaller slope inertia dominates and fluid is pushed to the outside of the channel. As in Arnold, Stokes, and Green[1], the balance between gravity and inertia may lead to multiple rotating cells of fluid but this does depend on the channel shape. For example, the secondary flow did not break into multiple cells for any choice of λ and ϵ for channels with parabolic cross-section or having a bottom of constant positive slope from inside to outside.

In fact we have found that the shape of the cross-section has a much stronger influence on the breakup of the secondary flow than do the downwards slope or curvature parameters, λ and ϵ. Just a small defect in the cross-sectional geometry may cause a breakup of the secondary flow. If, instead of a rectangular channel, the bottom slopes slightly downwards from inside to outside or there is a small bump in the channel bottom this will, for some choices of λ, ϵ and flux Q mean a secondary flow with two rotating cells instead of a single rotating cell. A bump in an otherwise parabolic cross-section also causes the secondary flow to break into two cells and we have numerical evidence that N sufficiently large bumps in the channel surface results in $N + 1$ rotating cells. The secondary velocity profile is relatively sensitive to the channel cross-sectional shape. However, the free-surface profile is far less sensitive. Bumps with height roughly 5-10% of the fluid depth are sufficient, in some cases, to cause a break-up of the flow into multiple rotating cells while the free-surface profile changes little. This finding is potentially important to particle segregation in spiral separators because it suggests that defects in or damage to the channel, or a build-up of solid material adhering to the channel base, along a long length of the channel, may significantly affect the secondary flow, which is believed to play an important role in the separation characteristics. Of course, imperfections in the channel geometry are most likely to be localised and may not, therefore, have much impact on particle segregation. To determine how far downstream any effects on the flow are likely to persist will require solution of the particulate flow problem in a channel whose shape varies with distance along the centreline (*i.e.* H, and therefore the flow, would be a function of β). This is left for future work.

ACKNOWLEDGMENTS

The asymptotic solution (36) to the small-torsion, small-curvature tick-shaped channel with positive bottom slope was first obtained by S.K. Wilson and B.R. Duffy (University of Strathclyde) as part of collaborative work with YMS on helically wound non-rectangular channels in the small curvature and small torsion limits, which has not been previously published. The authors also thank S. K. Wilson and B. R. Duffy for helpful comments on this work. We gratefully acknowledge funding from an Australian Postgraduate Award to DJA, an Australian Research Council Discovery Early Career Researcher Award (DE130100031) to JEFG and an Australian Research Council Discovery Project (DP160102021) to YMS.

[1] D. J. Arnold, Y. M. Stokes, and J. E. F. Green, "Thin-film flow in helically-wound rectangular channels of arbitrary torsion and curvature," J. Fluid Mech. **764**, 76–94 (2015).
[2] D. Gammack and P. E. Hydon, "Flow in pipes with non-uniform curvature and torsion," J. Fluid Mech. **433**, 357–382 (2001).
[3] D. G. Lynch, S. L. Waters, and T. J. Pedley, "Flow in a tube with non-uniform time-dependent curvature: governing equations and simple examples," J. Fluid Mech. **323**, 237–265 (1996).

ACCEPTED MANUSCRIPT

This manuscript was accepted by Phys. Fluids. Click here to see the version of record.

[4]L. Zabielski and A. J. Mestel, "Steady flow in a helically symmetric pipe," J. Fluid Mech. **370**, 297–320 (1998).
[5]D. Manoussaki and R. S. Chadwick, "Effects of geometry on fluid loading in a coiled cochlea," SIAM J. Appl. Math. **61**, 369–386 (2000).
[6]A. B. Holland-Batt, "A quantitative model of the motion of particles in the RSM/Mintek on-stream particle size analyser," Powder Technol. **11**, 11–25 (1975).
[7]A. B. Holland-Batt, "Spiral separation: theory and simulation," Trans. Instn. Min. Metall. (Sect. C: Mineral Process. Extr. Metall.) **98**, C46–C60 (1989).
[8]A. B. Holland-Batt, "Some design considerations for spiral separators," Miner. Eng. **8**, 1381–1395 (1995).
[9]A. B. Holland-Batt, "The dynamics of sluice and spiral separators," Miner. Eng. **8**, 3–21 (1995).
[10]A. B. Holland-Batt, "A method for the prediction of the primary flow on large diameter spiral troughs," Miner. Eng. **22**, 352–356 (2009).
[11]A. B. Holland-Batt and P. N. Holtham, "Particle and fluid motion on spiral separators," Miner. Eng. **4**, 457–482 (1991).
[12]H. W. Hou, M. E. Warkiani, B. L. Khoo, Z. R. Li, R. A. Soo, D. S.-W. Tan, W.-T. Lim, J. Han, A. A. S. Bhagat, and C. T. Lim, "Isolation and retrieval of circulating tumor cells using centrifugal forces," Scientific reports **3** (2013).
[13]P. N. Holtham, "Flow visualisation of secondary currents on spiral separators," Miner. Eng. **3**, 279–286 (1990).
[14]P. N. Holtham, "Primary and secondary fluid velocities on spiral separators," Miner. Eng. **5**, 79–91 (1992).
[15]D. Boucher, Z. Deng, T. Leadbeater, R. Langlois, M. Renaud, and K. E. Waters, "PEPT studies of heavy particle flow within a spiral concentrator," Miner. Eng. **62**, 120–128 (2014).
[16]D. Boucher, Z. Deng, T. Leadbeater, R. Langlois, and K. E. Waters, "Speed analysis of quartz and hematite particles in a spiral concentrator by PEPT," Miner. Eng. (2015).
[17]J. Wang and J. Andrews, "Numerical simulations of liquid flow on spiral concentrators," Miner. Eng. **7**, 1363–1385 (1994).
[18]B. W. Matthews, C. A. J. Fletcher, A. C. Partridge, and S. Vasquez, "Computations of curved free surface water flow on spiral concentrators," J. Hydraul. Eng. **125**, 1126–1139 (1999).
[19]Y. M. Stokes, "Flow in spiral channels of small curvature and torsion," in *IUTAM symposium on free surface flows*, Fluid mechanics and its applications, Vol. 62, edited by A. C. King and Y. D. Shikhmurzaev (Kluwer Academic Publishers, 2001) pp. 289–296.
[20]B. W. Matthews, C. A. J. Fletcher, and A. C. Partridge, "Computational simulation of fluid and dilute particulate flows on spiral concentrators," Appl. Math. Model. **22**, 965–979 (1998).
[21]Y. M. Stokes, B. R. Duffy, S. K. Wilson, and H. Tronnolone, "Thin-film flow in helically wound rectangular channels with small torsion," Phys. Fluids **25**, 083103 (2013).
[22]M. Bowen and J. R. King, "Dynamics of a viscous thread on a non-planar substrate," J. Engng. Math. **80**, 39–62 (2012).
[23]D. Holland, B. R. Duffy, and S. K. Wilson, "Thermocapillary effects on a thin viscous rivulet draining steadily down a uniformly heated or cooled slowly varying substrate," J. Fluid Mech. **441**, 195–221 (2001).
[24]S. K. Wilson and B. R. Duffy, "On the gravity-driven draining of a rivulet of viscous fluid down a slowly varying substrate with variation transverse to the direction of flow," Phys. Fluids **10**, 13–22 (1998).
[25]S. K. Wilson and B. R. Duffy, "A rivulet of perfectly wetting fluid draining steadily down a slowly varying substrate," IMA J. Appl. Math. **70**, 293–322 (2005).
[26]S. Lee, Y. M. Stokes, and A. Bertozzi, "Behaviour of a particle-laden flow in a spiral channel," Phys. Fluids **26** (2014).

ACCEPTED MANUSCRIPT